JACS
JOURNAL OF THE AMERICAN CHEMICAL SOCIETY

Article

Carbon-Dipyrromethenes: Bright Cationic Fluorescent Dyes and Potential Application in Revealing Cellular Trafficking of Mitochondrial Glutathione Conjugates

Hongxing Zhang, Jing Liu, Yuan-Qiang Sun, Mengxing Liu, and Wei Guo

J. Am. Chem. Soc., **Just Accepted Manuscript** • DOI: 10.1021/jacs.0c06916 • Publication Date (Web): 18 Sep 2020

is published by the American Chemical Society. 1155 Sixteenth Street N.W., Washington, DC 20036

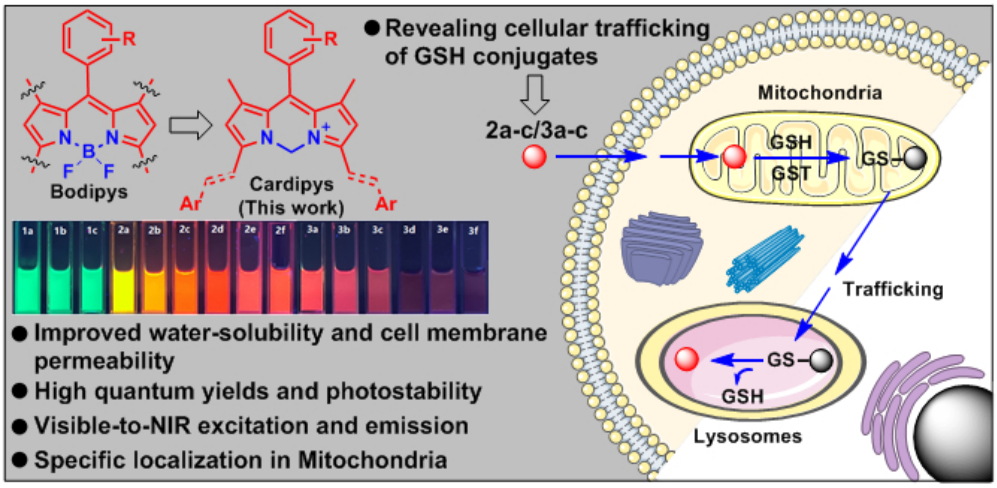
R
N
B
N
F
F
Bodipys
R
N
N+
Ar
Cardipys
(This work)
Ar
1a
1b
1c
2a
2b
2c
2d
2e
2f
3a
3b
3c
3d
3e
3f
● Revealing cellular trafficking of GSH conjugates
2a-c/3a-c
Mitochondria
GSH
GST
GS
Trafficking
GS
GSH
Lysosomes
● Improved water-solubility and cell membrane permeability
● High quantum yields and photostability
● Visible-to-NIR excitation and emission
● Specific localization in Mitochondria

Carbon-Dipyrromethenes: Bright Cationic Fluorescent Dyes and Potential Application in Revealing Cellular Trafficking of Mitochondrial Glutathione Conjugates

Hongxing Zhang,† Jing Liu,†,* Yuan-Qiang Sun,‡ Mengxing Liu,† and Wei Guo†,*

†*School of Chemistry and Chemical Engineering, Shanxi University, Taiyuan 030006, China.* ‡*College of Chemistry and Molecular Engineering, Zhengzhou University, Zhengzhou 450001, China.*

ABSTRACT: Boron-dipyrromethenes (Bodipys), since first reported in 1968, have emerged as a fascinating class of dyes in the past few decades due to their excellent photophysical properties including bright fluorescence, narrow emission bandwidth, resistance to photobleaching, and environment insensitivity. However, typical Bodipys are highly lipophilic, which often results in the nonfluorescent aggregates in aqueous solution, and also severely limits their bioavailability to cells and tissues. In this work, based on a simple one-atom B→C replacement in Bodipy scaffold, we present a new class of carbon-dipyrromethenes (Cardipys for short) fluorescent dyes with tunable emission wavelengths covering the visible and near-infrared regions. These Cardipys not only retain excellent photophysical properties of conventional Bodipys, but also show improved water solubility and photostability due to their cationic character. Moreover, the cationic character also makes them extremely easy to penetrate cell membrane and specifically accumulate into mitochondria without resorting to any mitochondria-targeted groups. Interestingly, several Cardipys bearing active styryl groups could serve as fluorescent indicators to map cellular trafficking of the glutathione conjugates produced within mitochondria under the catalysis of glutathione S-transferase (GST), thus showing potentials in either exploring the detoxification mechanism of mitochondrial GST/GSH system or evaluating the drug resistance of cancer cells that is closely related with GST activity.

INTRODUCTION

Fluorescence imaging technique, as a nonionizing radiation method, is one of the most powerful cellular biology tools to study biological phenomena due to the visualization, noninvasiveness, sensitivity, real-time monitoring, and high spatiotemporal resolution. With the technique, imaging and tracing of various biological species and dynamic biological events in living cells or whole organisms could be achieved, largely advancing our understanding on biological systems and also facilitating the drug development, clinical diagnosis, and disease treatment.[1-5] However, compared with the rapid progress of fluorescence technique in recent years, the development of fluorescent dyes that simultaneously have good biocompatibility, high fluorescence brightness (ε·Φ), and long-term photostability still remains an unmet challenge, necessitating more studies and greater efforts to exploit new or modify existing fluorophores to improve their photophysical properties and biocompatibility.[6-16]

Among various fluorophores, boron-dipyrromethenes (Bodipys) (Scheme 1A), since first reported by Treibs and Kreuzer in 1968,[17] have emerged as a fascinating class of fluorescent dyes in the past few decades due to their excellent photophysical properties including bright fluorescence, narrow emission bandwidth, resistance to photobleaching, and environment insensitivity.[18-21] Moreover, the rich chemistry of Bodipys also allows a large number of red to near-infrared (NIR) Bodipy derivatives to be constructed to improve tissue penetration depth and signal-to-background ratio and reduce photodamage.[22,23] As a result, Bodipys and their red to NIR derivatives have widely been utilized as fluorescent labels and indicators for various bioimaging applications.[18-23] What's more, due to the high singlet oxygen ($^1O_2$) quantum yield, large light-dark toxicity ratios, high photostability, and facile structural modification, the Bodipy-based photosensitizers have been recognized to be the most potential candidates for photodynamic therapy except conventional porphyrin derivatives.[24-26] Despite all of these advantages, typical Bodipys and their derivatives, however, are inherently lipophilic and thus have poor water solubility, which often results in the nonfluorescent aggregates in aqueous solution and also seriously limits their bioavailability to cells and tissues.[27-35] Moreover, the strong lipophilicity also increases their tendency to accumulate into cellular lipophilic components, thereby decreasing the contrast between specific and nonspecific staining and in turn affecting the accurate assessment of cellular events of interest.[29] This is why many strategies had to be employed to endow Bodipys with appropriate water solubility, e.g., through addition of hydrophilic groups, such as sulfonates, phosphonates, carbohydrates, and polyethylene glycols,[27-35] or formation of water-soluble nanoparticles via polymer encapsulation or host-guest

interactions.[25,36-40] However, the complex synthesis, reduced sites for further functionalization, decreased cell membrane permeability caused by the attached ionic groups, and possible dye leakage from nanoparticles may make these methods complicated in some cases. In this work, by applying an one-atom B→C replacement strategy to conventional Bodipy scaffolds, we present a new class of cationic fluorescent dyes, i.e. carbon-dipyrromethenes (Cardipys for short), with the absorption and emission wavelengths covering the visible and near-infrared regions (Scheme 1B). Importantly, these Cardipys not only retain the excellent photophysical properties of conventional Bodipys such as bright fluorescence and narrow emission bandwidths, but also show improved water solubility and photostability due to their cationic character. Moreover, the cationic character also makes them extremely easy to penetrate cell membrane and accumulate into mitochondria. Furthermore, several Cardipys bearing active styryl groups could act as fluorescent indicators to map the cellular trafficking of glutathione conjugates of mitochondrial toxic electrophiles produced under the catalysis of glutathione S-transferase (GST), thus showing great potentials in either exploring the detoxification mechanism of mitochondria or evaluating the drug-resistance of cancer cells to anticancer drugs.

Scheme 1. Design and synthesis of Cardipys 1-3.

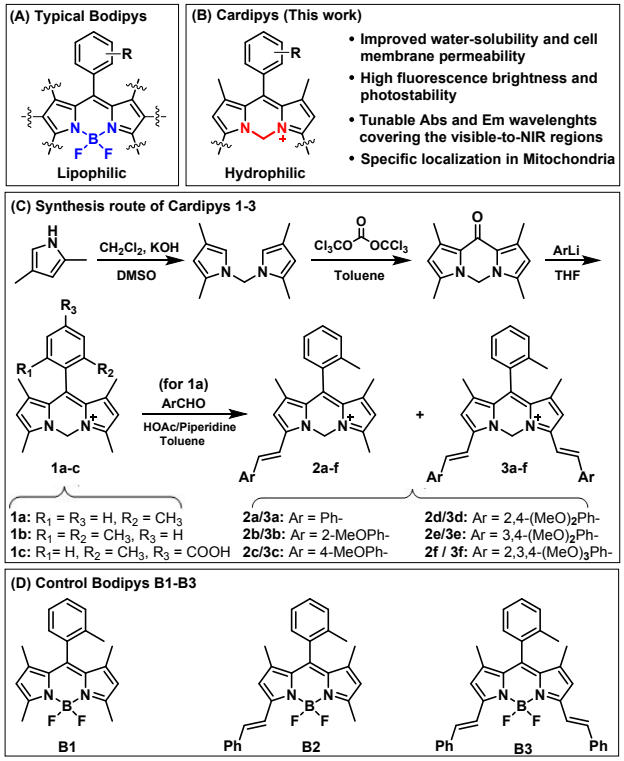

RESULTS AND DISCUSSION

Design and Synthesis. Our design originates from the understanding of the widely used carborhodamine cationic dyes that were constructed by an one-atom O→C replacement on rhodamine scaffolds.[41,42] We envisioned that the one-atom B→C replacement should also be applicable for Bodipy scaffolds to achieve Cardipys with cationic character. With this consideration in mind, we set out to design and synthesize Cardipys **1a-c** by a simple three-step procedure starting from the commercial 2,4-dimethylpyrrole. As shown in Scheme 1C, the treatment of 2,4-dimethylpyrrole with CH_2Cl_2 in the presence of KOH provided N,N'-dipyrrolylmethane; subsequent reaction of N,N'-dipyrrolylmethane with triphosgene in refluxing toluene provided the key intermediate N,N'-dipyrrolyl ketone; finally, the treatment of the ketone with aromatic lithium reagents gave Cardipys **1a-c**. Note that Cardipy **1c** was designed to possess a *meso*-substituted benzoic acid group, making it easy to be conjugated to biomolecules via amide bond formation.[43] Further, with Cardipy **1a** as starting material, we simultaneously obtained monostyryl- and distyryl-substituted Cardipys **2a-f** and **3a-f** via Knoevenagel reaction with various aromatic aldehydes in one pot. These π-conjugation expanded Cardipys were expected to have red to NIR excitation and emission, thus being more favorable for bioimaging applications given the advantages of light in the wavelength range, including less photodamage to cells, improved tissue penetration depth, and reduced interference from biomolecular autofluorescence. Detailed synthesis procedures and characteristic data of these Cardipys are shown in Supporting Information.

Aqueous Solubility and Photostability. With these Cardipys in hand, we first compared the aqueous solubility of Cardipys **1a-3a** (as representatives of the above three types of Cardipys) with that of their Bodipy analogues B1-B3 using absorption spectra. As shown in Figure 1A, Cardipys **1a-3a** all showed almost identical absorption spectra profiles in both CH_3CN and PBS (or a 8:2 mixture of PBS/CH_3CN, for **3a**) with essentially unchanged peak/shoulder ratio; in contrast, control Bodipys B1-B3 only showed sharp absorbance in CH_3CN, whereas in PBS or a mixture of PBS/CH_3CN (for B3), these peaks were obviously red-shifted and broadened along with a decreased peak/shoulder ratio, a typical characteristic of aggregation.[28,32] The results clearly indicate that Cardipys have higher aqueous solubility than typical Bodipys due to their cationic character. Moreover, the absorption titration studies further revealed that in PBS or PBS/CH_3CN (8:2, for **3a**), the concentration of Cardipys **1a-3a** could reach up to 40 μM (data not shown), which is sufficient for most bioimaging applications. Not only that, Cardipys **1a-3a** were also found to have higher photostability than that of Bodipys B1-B3 when continuously irradiated by a Xe lamp for 10 min, although the latters had better photostability than the widely used cyanine dyes Cy5.5 and Cy7 (Figure 1B). In fact, the higher photostability of Cardipys **1a-3a** than that of their Bodipy analogues could also be attributed to the cationic character that decreases their π-electron intensity and increases the oxidation potentials to protect against photobleaching.[44] Taken together, these results indicate that the cationic character endows Cardipys with the improved water-solubility and photostability relative

to those of their Bodipy analogues, both of which are indeed highly desirable for bioimaging applications.

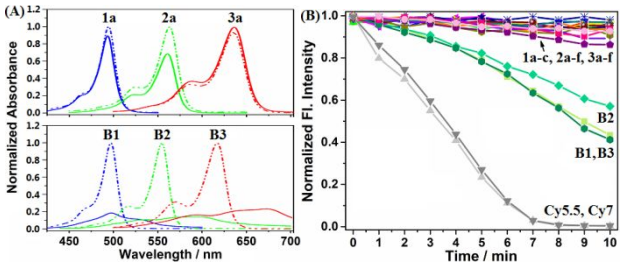

Figure 1. (**A**) Absorption spectra of **1a-3a** and **B1-B3** (4 μM) in CH3CN (dashed line) and PBS or PBS/CH3CN 8/2 (for **3a** and **B3**) (solid line). (B)Fluorescence intensity changes of **1a-3a**, **B1-B3**, Cy5.5, and Cy7 in CH3CN continuously irradiated by a Xe lamp for 10 min.

Photophysical and Electrochemical Properties. Subsequently, we tested the photophysical properties of all of these Cardipys shown in Scheme 1C, including **1a-c**, **2a-f**, and **3a-f**, in representative solvents. The absorption and emission spectra of these Cardipys are shown in Figure 2A,B and Figure S1, and the corresponding photophysical data are listed in Table 1. As can be seen, for Cardipys **1a-c**, their absorption and emission maxima were located at around 495 nm and 510 nm, respectively, which are similar to those of typical Bodipys, indicating that the one-atom B→C replacement has little effect on their absorption and emission wavelengths. For Cardipys **2a-f** bearing a styryl group, their absorption and emission maxima were largely red-shifted to the wavelength ranges of 561–607 nm and 577–646 nm, respectively, due to the expanded π-conjugation. For Cardipys **3a-f** bearing two styryl groups, the red shifts in absorption (635–705 nm) and emission maxima (653–742 nm) were more remarkable, which essentially fall into the sought-after biological NIR window, due to their more expanded π-system. Notably, these mono- and distyryl-substituted Cardipys, except **2a** and **3a**, had larger Stokes shifts (23–49 nm) than **1a-c** (ca. 16 nm), consistent with the improved intramolecular charge transfer (ICT) property due to the presence of the electron-donating methoxy group. Importantly, almost all of these Cardipys showed the large extinction coefficients and high fluorescence quantum yields, indicating that the one-atom B→C replacement in Bodipy scaffolds scarcely compromises their photophysical properties. Moreover, the high fluorescence quantum yields of these Cardipys were also reflected by the brilliant fluorescence of their solution under a 365 nm UV lamp (Figure 2C), except **3d-f** whose fluorescence is out of the wavelength range visible by naked eye. Taken together, these results reveal that Cardipys are a new class of water-soluble, bright, and photostable fluorescent dyes with absorption and emission wavelengths covering visible and NIR regions.

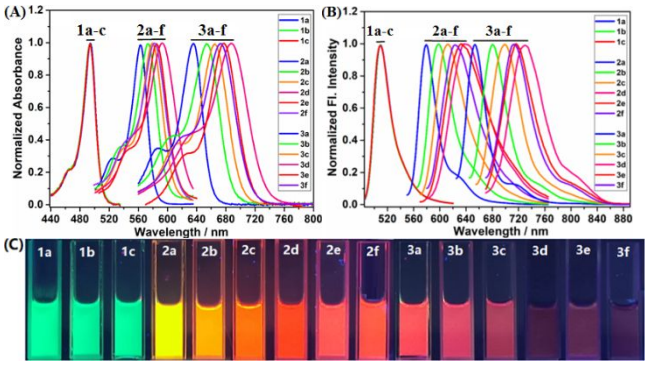

Figure 2. (A,B) Absorption and emission spectra of **1a-c**, **2a-f**, and **3a-f** in CH_3CN. (C) Fluorescence colors of **1a-c**, **2a-f**, and **3a-f** in CH_3CN under a 365 nm UV lamp. Note that for **3d-f**, their fluorescence is out of the wavelength range visible by naked eyes.

Table 1 Photophysical properties of Cardipys 1a-c, 2a-f, and 3a-f in CH_2Cl_2, CH_3CN, and PBS, respectively.

Dyes	Sol.	$\lambda_{abs}/\lambda_{em}$ (nm)	Stokes shift	ε (M^{-1} cm^{-1})	Φ	τ (ns)
1a[a]	CH2Cl2	497/511	14	75600	1.03±0.05	
	CH_3CN	494/510	16	57700	0.93±0.02	5.84
	PBS	493/509	16	62500	0.91±0.01	
1b[a]	CH2Cl2	496/511	15	62500	0.96±0.04	
	CH3CN	494/509	15	46800	0.97±0.08	7.53
	PBS	493/509	16	56800	0.98±0.05	
1c[a]	CH2Cl2	498/514	16	47400	0.68±0.04	
	CH3CN	496/512	16	46000	0.61±0.01	4.59
	PBS	494/510	16	46500	0.84±0.04	
2a[b]	CH2Cl2	571/587	16	102700	0.53±0.09	
	CH3CN	563/579	16	81700	0.57±0.03	7.28
	PBS	561/577	16	69400	0.58±0.03	
2b[c]	CH2Cl2	583/607	24	77900	1.01±0.05	
	CH3CN	573/598	25	57800	1.02±0.07	5.99
	PBS	570/593	23	41400	0.96±0.04	
2c[c]	CH2Cl2	593/622	29	78800	0.73±0.09	
	CH3CN	580/612	32	70600	0.82±0.05	5.32
	PBS	573/605	32	49500	0.77±0.03	
2d[c]	CH2Cl2	607/646	39	73100	0.43±0.01	
	CH3CN	593/642	49	57600	0.38±0.01	4.13
	PBS	584/633	49	38900	0.23±0.05	
2e[c]	CH2Cl2	600/641	41	74500	0.68±0.09	
	CH3CN	585/631	46	66500	0.33±0.07	2.28
	PBS	576/617	41	60700	0.05±0.01	
2f[c]	CH2Cl2	596/633	37	68700	0.71±0.03	
	CH3CN	582/624	42	58700	0.48±0.07	2.95
	PBS	575/609	34	45000	0.23±0.01	
3a[c]	CH2Cl2	647/665	18	91500	0.43±0.01	
	CH3CN	635/653	18	83200	0.42±0.05	5.51
	80% PBS	636/654	18	49500	0.36±0.03	
3b[d]	CH2Cl2	670/696	26	80100	0.95±0.03	
	CH3CN	654/681	27	68600	0.93±0.07	4.16
	80% PBS	653/680	27	59700	0.57±0.01	
3c[d]	CH2Cl2	684/713	29	92300	0.65±0.01	
	CH3CN	665/699	34	92400	0.80±0.04	4.05
	80% PBS	664/698	34	72300	0.55±0.01	
3d[d]	CH2Cl2	705/742	37	85000	0.52±0.03	
	CH3CN	687/730	43	70800	0.39±0.03	3.00
	80% PBS	667/708	41	57800	0.19±0.01	
3e[d]	CH2Cl2	695/728	33	95500	0.49±0.01	
	CH3CN	678/716	38	77900	0.48±0.04	3.00
	80% PBS	670/710	40	75500	0.32±0.03	
3f[d]	CH2Cl2	690/725	35	79500	0.47±0.03	
	CH3CN	673/714	41	81000	0.48±0.01	3.21

80% PBS	667/708	41	69000	0.49±0.04

Reference compounds for determining fluorophores quantum yields. [a]Fluorescein (Φ_f = 0.95 in 0.1 M NaOH) for **1a-c**; [b]rhodamine B (Φ_f = 0.49 in ethanol) for **2a**; [c]cresyl violet (Φ_f = 0.58 in ethanol) for **2b-f** and **3a**; [d]Cy5.5 (Φ_f = 0.23 in PBS) for **3b-f**. Note that 80% PBS refers to PBS/CH_3CN (v/v = 8:2).

In addition, we also performed cyclic voltammetry on Cardipy **1a** and Bodipy **B1** (as representatives) to evaluate their difference in redox properties. As shown in Figure S2, compared with Bodipy **B1**, Cardipy **1a** showed more positive reduction potential (–0.807 V/–0.756 V for **B1**/**1a**), indicating that it is easier for **1a** to be reduced, consistent with its cationic character. Based on these data and coupled with their absorption spectra, we calculated the HOMO and LUMO levels of **B1**/**1a** and confirmed that the HOMO and LUMO levels of **1a** are lower than those of Bodipy **B1** (For **B1**, HOMO/LUMO = –6.295/–3.933 eV; For **1a**, HOMO/LUMO = –6.350/–3.984 eV) (Figure S2), also consistent with the cationic character of **1a**.

Bioimaging Applications. Encouraged by the above results, we set out to test the cellular imaging abilities of these Cardipys in A549 cells using confocal laser-scanning microscope (CLSM). The obtained results revealed that all of them, except **1c** that contains a carboxylate anion and thus is cell membrane-impermeable, could penetrate cell membrane within 30 min to give rise to bright visible-to-NIR intracellular fluorescence in term of their emission wavelengths (Figure 3A and Figure S3). By comparison, control Bodipys B2 and B3 were poorly and hardly cell membrane-permeable, respectively, mainly due to their low solubility in the cell-culture medium, while B1 could penetrate cell membrane due to its small molecule size (Figure 3B). Obviously, the cationic character endows these Cardipys not only with good compatibility with cell culture fluid, but also with strong ability to penetrate the negatively charged cell membrane. In this regard, Cardipys appear to be more suitable for bioimaging studies than conventional Bodipys.

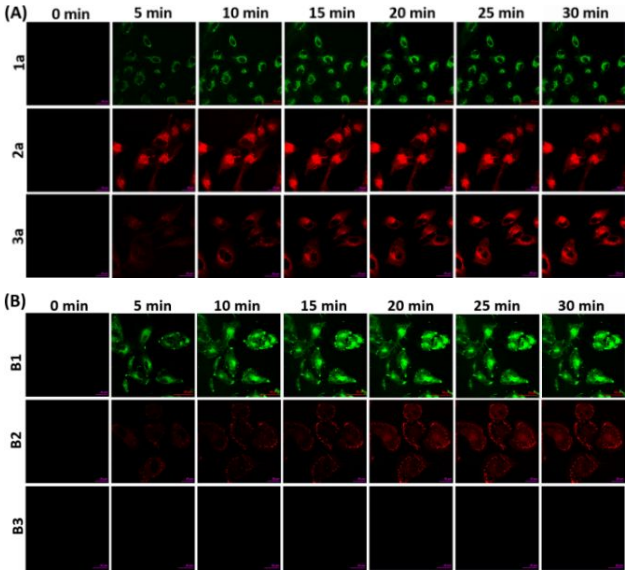

Figure 3. Time-lapse fluorescence images of A549 cells treated with cardipys **1a**-**3a** (0.2 μM) (A) and control compounds B1-B3 (0.2 μM) (B), respectively. Images were obtained in the indicated time points. For **1a**-**3a**, emissions were collected at 500–550 nm (λ_{ex} = 488 nm), 570–650 nm (λ_{ex} = 561 nm), and 640–750 nm (λ_{ex} = 633 nm), respectively; For B1-B3, at 500–600 nm (λ_{ex} = 488 nm), 570–700 nm (λ_{ex} = 561 nm), and 640–750 nm (λ_{ex} = 633 nm), respectively.

Also, we tested the cytotoxicity of these Cardipys by CCK8 assays. The obtained results revealed that all of them have low cytotoxicity in the concentration range of 0–5 μM (cell viability: >85% for 24 h or longer incubation time, Figures S4 and S5), which is superior to the widely used and commercial Cy5 and Cy7. Moreover, histological hematoxylin and eosin (H&E) staining of various organs of the mice pretreated with representative Cardipys (**1a**-**3a**) for 24 h, 48 h, and 72 h, respectively, showed normal tissue morphology (Figure S6), indicating that they do not significantly cause tissue damages. Notably, due to the high fluorescence brightness, these Cardipys could be used at a very low concentration (0.2 μM) in the cellular imaging assays, and in this case, all of them showed the negligible cytotoxicity (cell viability: ~100%).

Further, we studied the cellular uptake mechanism of Cardipys with **2b** as a representative. In these assays, A549 cells were first incubated with **2b** at 37 °C and 4 °C, respectively, to determine whether the dye enters cells via endocytosis pathway or passive diffusion pathway. As shown in Figure S7, the bright intracellular fluorescence could be observed in both cases, which, coupled with the ability of rapidly penetrating cell membrane, suggests that **2b** could be internalized by cells via energy-independent passive diffusion pathway, rather than energy-dependent endocytosis pathway. The conclusion is also supported by the fact that endocytotic inhibitors chlorpromazine (clathrin inhibitor) and amiloride (actin inhibitor) did not obviously affect the cell uptake of **2b** (Figure S7). These results indicate that Cardipys could be taken up by cells by passive diffusion pathway, consistent with their good cell membrane permeability.

Given their cationic character, we further envisioned that these Cardipys should be able to specifically accumulate into mitochondria, as with those positively charged fluorescent dyes.[45,46] However, the subsequent co-staining assays revealed that they, except **1c** that is cell membrane-impermeable as mentioned previously, have two different types of subcellular distributions. As shown in Figure 4A and Figure S8, for Cardipys **1a**,**b**/**2d-f**/**3d-f**, the specific accumulation in mitochondria was observed even in a lengthened incubation time of 1 h, consistent with their cationic character. To our surprise, Cardipys **2a-c**/**3a-c**, as shown in Figure 4B and Figure S9, exhibited a gradual mitochondria-to-lysosome translocation within 30 min, as highlighted by their initial co-localization with MitoTracker but not with LysoTracker (video S1), and subsequent co-localization with LysoTracker but not with MitoTracker (video S2). To exclude the effect of subjective factors, we further studied their mitochondria-to-lysosome translocation with **2b** as a representative using flow cytometry combining with CLSM. As shown in

Figure S10, the high percentage of the double positive cells (> 99%, total events are 5000) in flow cytometry analysis revealed that **2b** could be internalized into cells together with MitoTracker or LysoTracker. Subsequently, we performed fluorescence imaging of A549 cells co-stained with **2b** and MitoTracker or LysoTracker under CLSM equipped with a 10× objective lens (in this case a large number of cells were observed). And then, two separate cells were randomly selected for exploring the mitochondria-to-lysosome translocation of **2b** with a 64×oil-immersion objective lens (in this case mitochondria and lysosomes were clearly discernable). As shown in Figure S11, the time-lapse fluorescence imaging revealed that the mitochondria-to-lysosome translocation of **2b** occurred in both the two cells, indicating that the mitochondria-to-lysosome translocation of **2a-c/3a-c** should be a general phenomenon, rather than a subjective judgment.

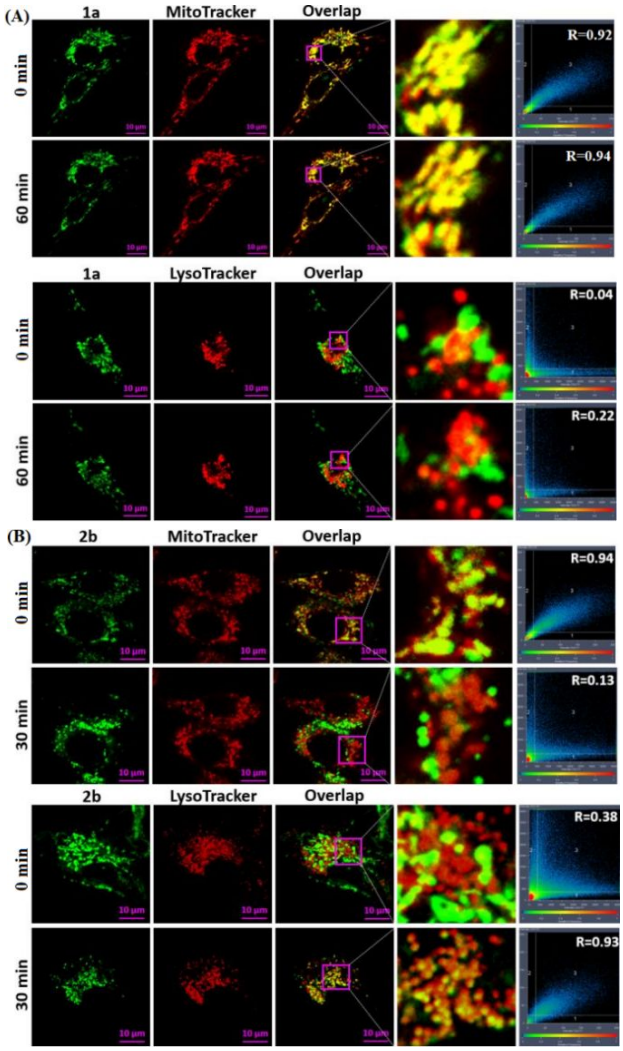

Figure 4. (A) Time-lapse fluorescence images of A549 cells co-stained with **1a** (0.2 μM)/MitoTracker Deep Red (0.2 μM) or **1a** (0.2 μM)/LysoTracker Deep Red (0.2 μM), indicating the stable mitochondria localization of **1a**,**b**/**2d-f**/**3d-f** with **1a** as a representative. (B) Time-lapse fluorescence images of A549 cells co-stained with **2b** (0.2 μM)/MitoTracker Deep Red (0.2 μM) or **2b** (0.2 μM)/LysoTracker Deep Red (0.2 μM), indicating the mitochondria-to-lysosome translocation of **2a-c**/**3a-c** with **2b** as a representative. For **1a** and **2b**, emissions were collected at 490–550 nm (λ_{ex} = 488 nm) and 570–630 nm (λ_{ex} = 561 nm), respectively; for both MitoTracker and LysoTracker Deep Red, at 640–750 nm (λ_{ex} = 633 nm).

Initially, we intuitively attributed the mitochondria-to-lysosome translocation of **2a-c**/**3a-c** to mitochondrial autophagy (Mitophagy), a normal cell response to remove damaged mitochondria by fusing with lysosomes.[47] However, the fact that the mitochondria labeled by MitoTracker did not fuse with the lysosomes lighted up by the transferred **2a-c**/**3a-c** ruled out the possibility. Exactly what causes the translocation of **2a-c**/**3a-c**? Considering that lysosomes are responsible for the degradation and recycling of cellular and extracellular components,[48,49] we surmised that the mitochondria-to-lysosome translocation of **2a-c**/**3a-c** is probably implicated in the lysosomal disposal of the compromised mitochondrial biomolecules. However, the questions are how **2a-c**/**3a-c** inactivate the mitochondrial biomolecules and which biomolecules are inactivated by them.

Inspired by a recent report by Cosa and coworkers on a Bodipy-acrolein fluorescent probe that could map cellular trafficking of the compromised mitochondrial proteins via Michael addition of its acrolein group with cysteine (Cys) residue of these proteins,[50] we reasoned that a similar case could also occur for Cardipys **2a-c**/**3a-c**, because their cationic Cardipy core probably activates the adjacent styryl group to behave like a Michael acceptor to be attacked by the Cys-containing biomolecules. In fact, the hypothesis was supported by the stable mitochondrial localization of either Cardipys **1a**,**b** bearing no styryl group or Cardipys **2d-f**/**3d-f** bearing less active 2,4-dimethoxy-, 3,4-dimethoxy-, and 2,3,4-trimethoxy-substituted styryl groups, respectively (Figure S8) (Note that, methoxy is a strong electron-donating group that could lower the electrophilicity of styryl group by increasing its electron density). That is to say, the mitochondria-to-lysosome translocation of **2a-c**/**3a-c** is probably initially caused by their Michael addition with Cys-containing biomolecules, such as glutathione (GSH, the most abundant intracellular biothiol) (Figure 5A), since the styryl groups of these Cardipys contain no or only a methoxy group and thus are more reactive than **2d-f**/**3d-f**. To support the hypothesis, we tested the dependency of the mitochondria-to-lysosome translocation of **2b** (as a representative) on biothiol level within cells. As shown in Figure S12, when A549 cells were pretreated with N-ethylmaleimide (NEM) to deplete intracellular biothiols,[51] the mitochondria-to-lysosome translocation of **2b** was completely blocked as revealed by its stable mitochondria localization within 30 min, strongly indicating that the mitochondria-to-lysosome translocation of **2a-c**/**3a-c** is probably caused by biothiols.

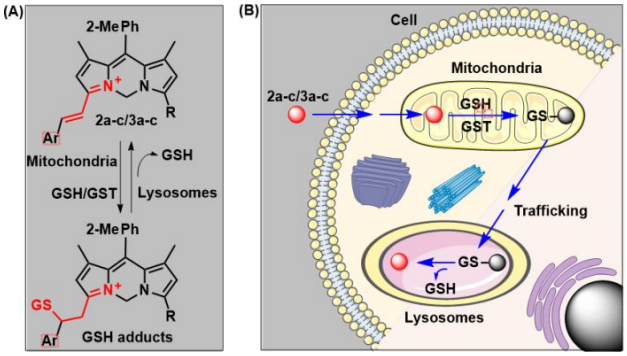

Figure 5. (A) Proposed Michael addition of **2a-c**/**3a-c** with GSH under the catalysis of GST within mitochondria as well as the retro-Michael addition of the GSH adducts that regenerates **2a-c**/**3a-c** and GSH within lysosomes. (B) Schematic illustration of the cellular trafficking of **2a-c**/**3a-c** from mitochondria to lysosomes.

To figure out which biothiol is involved in the mitochondria-to-lysosome translocation of **2a-c**/**3a-c**, we tested the reactivity of **2a** toward various biothiols, including Cys, GSH, glutathione S-transferase (GST), thioredoxin (Trx), glutathione reductase (GR), and glutaredoxin (Grx), all of which play crucial roles in controlling redox balance to defend against oxidative stress,[52,53] in B-R buffer (pH = 8.0) at 37 °C by absorption spectra. Note that, the selection of pH = 8.0 is in order to simulate the weakly basic mitochondrial macroenvironment.[54] Unfortunately, none of them could induce obvious absorption spectra change of **2a** (Figure S13), meaning that they should not be the molecular targets of **2a**. Further, selenocysteine (Sec) and thioredoxin reductase (TrxR) were also found to fail to react with **2a** in the condition, although both of them contain a more nucleophilic selenol group (Figure S13).[55] To our delight, the addition of GST, a phase II detoxifying enzyme that catalyzes GSH conjugation with a wide variety of exogenous and endogenous electrophiles and thereby protects biomolecules from being damaged by these electrophiles,[56,57] to the mixture of **2a** and GSH resulted in a remarkable decrease of the initial absorption peak of **2a** at 561 nm and a simultaneous appearance of a blue-shift new absorption peak at 499 nm (Figure S14A), strongly indicating that GST could catalyze the reaction of GSH with **2a** to produce **2a**-GSH adduct. The conclusion could further be confirmed by HPLC-MS analysis of the reaction mixture of **2a**/GSH/GST, where only one new product was observed with mass-to-charge ratio (m/z) corresponding to **2a**-GSH adduct (Figure S14C). Similar absorption spectra changes were also observed for **2b** and **2c** in the same condition (Figure S15). Moreover, Cardipys **3a-c** were also expected to be able to undergo such reaction because they contain the same styryl groups to **2a-c**. These results are indeed consistent with the catalytic function of GST that can improve the nucleophilicity of the thiol group of GSH by lowering its pK_a from 9.0 to about 6.5,[58] and also consistent with the higher Michael receptor activity of **2a-c**/**3a-c** than that of **2d-f**/**3d-f**. Taken together, these results indicate that the mitochondria-to-lysosome translocation of **2a-c**/**3a-c** should be caused by the GST-catalyzed Michael addition of them with GSH as well as the subsequent cellular trafficking of the resulting GSH adducts (Figure 5).

Even so, it is still insufficient to explain the cellular imaging results, because, during the mitochondria-to-lysosome translocation process, we only observed the fluorescence changes of **2a-c**/**3a-c** that first decreased in mitochondria and then increased in lysosomes (Figures S9 and S16), and did not find any blue-shifted fluorescence of their GSH adducts either in mitochondria or lysosomes, although the latter is observable in chemical system (Figure S14B). We speculated that this is probably due to the rapid cellular trafficking of their GSH adducts as well as the quick lysosomal disposal of the adducts. To support the speculation, we performed the HPLC-MS analysis of the lysate of A549 cells pretreated with **2b** (as a representative) for 30 min (at this time point, the mitochondria-to-lysosome translocation has been finished). The obtained result demonstrated **2b** to be the only product (Figure S17), indicating that the **2b**-GSH adduct initially formed within mitochondria probably suffered from a retro-Michael addition to regenerate **2b** and GSH within lysosomes (Figure 5). Although the mechanism remains to be identified, a similar retro-Michael addition was also observed in the metabolic process of the GSH conjugate of 4-hydroxy-2-nonenal (HNE, a lipid-derived Michael receptor).[59] Based on these results, we proposed a possible mitochondria-to-lysosome translocation mechanism of **2a-c**/**3a-c**: they first localized in mitochondria due to the cationic character, and then conjugated with GSH under the catalysis of GST to form GSH adducts; the resulting GSH adducts rapidly migrated to lysosomes mediated by certain cellular trafficking mechanism, and then undergone a retro-Michael addition to regenerate **2a-c**/**3a-c** and GSH (Figure 5B).

Overall, the above assays indicate that the mitochondria-to-lysosome translocation of **2a-c**/**3a-c** observed in cellular imaging assays should be a result of the cellular trafficking of their GSH conjugates, which probably reflects the GST-mediated detoxifying pathway of mitochondrial lipid-derived electrophiles, such as various α,β-unsaturated carbonyl compounds produced endogenously in mitochondria as oxidation byproducts of polyunsaturated fatty acids and exerting toxic effects by alkylating protein and DNA.[50,60] In this sense, **2a-c**/**3a-c** should be promising as fluorescent indicators to probe the pathogenesis associated with the abnormal mitochondrial GST/GSH detoxifying system.

Potential Application in Evaluating Drug-Resistance of Cancer Cells. It is known that the development of drug resistance, i.e. the ability of cancer cells to acquire resistance to various drugs, is a major obstacle to anticancer treatments. Although the mechanisms underlying this resistance are multiple, the overexpression of GST and the high level of GSH in cancer cells have been recognized to be one of main reasons, because GST can promote GSH conjugation with anticancer drugs to lead to their deactivation and cellular removal before reaching targets.[61,62] In this context, we

envisioned that Cardipys **2a-c**/**3a-c** may have potential to act as fluorescent indicators to evaluate the drug resistance of cancer cells in term of their GST activity that was expected to be positively correlated with the mitochondria-to-lysosome translocation rates of **2a-c**/**3a-c**. With this consideration in mind, we tested the mitochondria-to-lysosome translocation of **2b** (as a representative) in both cancer cells and drug-resistant cancer cells. In the assays, we employed commercial LysoTracker as the endpoint reference of the translocation process. As shown in Figure 6A, in cancerous A549 cells, **2b** showed a gradual mitochondria-to-lysosome translocation that could be completed within 15 min, as indicated by the excellent overlap image of **2b** and LysoTracker (Pearson correlation coefficient R = 0.89) at the time point; by comparison, in the drug-resistant A549 cells (A549/ADM, obtained by continuous exposure of A549 cells to incrementally increasing concentrations of Adriamycin (ADM) over a period of 8 months), the translocation process of **2b** was largely accelerated and could be completed within 6 min (Figure 6B), consistent with the overexpression of GST in drug-resistant cancer cells.[63] In addition, we found that the mitochondria-to-lysosome translocation of **2b** could also be dramatically promoted when A549 cells were pretreated with anticancer drugs ADM, cisplatin, and gemcitabine (GEM) for 12 hr (Figure 6C-E), also consistent with the report that GST activity of cancer cells could be induced by anticancer drugs.[64] Thus, **2a-c**/**3a-c** could be used to examine the characteristics of cancer cells with the drug-resistance phenotype or potential, thus being promising as imaging tools either to explore the drug-resistant mechanisms of cancer cells or to screen anticancer agents that can prevent the development of drug resistance.

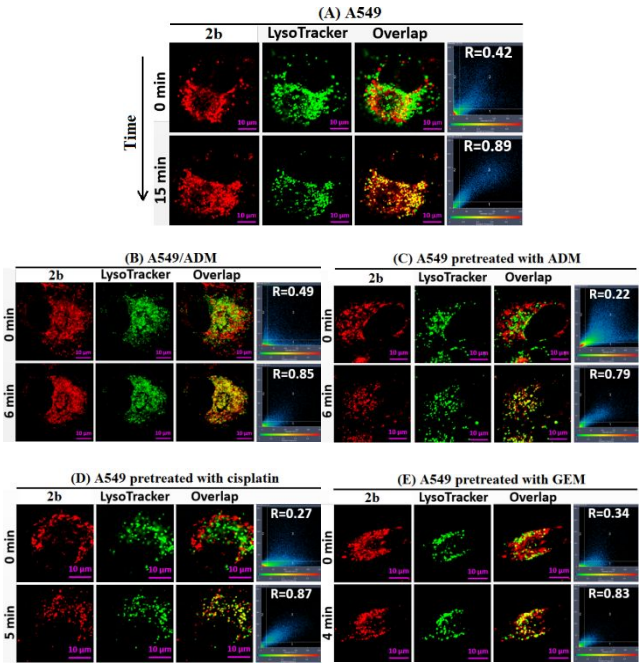

Figure 6. (A,B) Time-lapse fluorescence images of A549 cells and drug-resistant A549/ADM cells co-stained with LysoTracker Green DND 26 (0.2 μM) and **2b** (0.2 μM). (C-E) Time-lapse fluorescence images of A549 cells pretreated with anticancer drugs ADM (10 μM), cisplatin (5 μM), and GEM (10 μM) for 12 hr, and then treated with LysoTracker Green (0.2 μM) and **2b** (0.2 μM). The overlap images highlight the translocation of **2b** from mitochondria to lysosomes. For **2b**, emissions were collected at 570–630 nm (λ_{ex} = 561 nm); for both LysoTracker Green DND 26, at 490–560 nm (λ_{ex} = 488 nm).

Finally, to figure out whether the mitochondria-to-lysosome translocation of **2b** is also promoted by the high level of intracellular GSH, A549 cells were pretreated with 5 mM or 10 mM GSH ethyl ester (GSHee, a cell-permeant form of GSH that could increase intracellular GSH content)[65,66] and then treated with **2b** and MitoTracker or LysoTracker. The time-lapse fluorescence imaging showed that the mitochondria-to-lysosome translocation of **2b** was hardly speeded up when compared with the case in control cells without GSHee pre-treatment (Figure S18), strongly indicating that the mitochondria-to-lysosome translocation of **2b** is not influenced by the excessive intracellular GSH. This is indeed consistent with the dynamical character of enzyme-catalyzed reactions, i.e. the substrate saturation phenomenon, and also indicates that the mitochondria-to-lysosome translocation of **2b** is dominated by the activity of GST that is commonly overexpressed in cancer cells, especially the drug-resistant cancer cells.

CONCLUSIONS

In conclusion, on the basis of a simple one-atom B→C replacement strategy in Bodipy scaffold, we have developed a new class of cationic Cardipys fluorescent dyes with tunable absorption and emission wavelengths covering visible and near-infrared regions. These Cardipys not only inherit the excellent photophysical properties of conventional Bodipys, such as bright fluorescence, narrow emission bandwidth, and environment insensitivity, but also exhibited improved water solubility and photostability due to their cationic character. What's more, the cationic character also makes these Cardipys easy to penetrate cell membrane and specifically accumulate into mitochondria, thus showing potentials either as fluorescence imaging agents to explore mitochondria biofunctions or as candidates to develop photosensitizers for mitochondria-targeting photodynamic therapy. Furthermore, several Cardipys bearing active styryl groups were found to show a mitochondria-to-lysosome translocation upon entering into cells, which has been confirmed to be initiated by Michael addition of their styryl groups with GSH under the catalysis of GST. Importantly, the translocation probably reflects the detoxification pathway of the lipid-derived electrophiles (LDE) that are endogenously generated within mitochondrial membranes and have been indicated to be implicated in cellular toxicity and pathogenesis of neurodegenerative diseases and atherosclerosis, and so on.[67,68] Thus, these Cardipys should hold the potentials as fluorescent indicators to probe the pathogenesis that is closely related to the abnormal mitochondrial GST/GSH detoxifying system. Also, we found that the mitochondria-to-lysosome translocation of these Cardipys could greatly be promoted in the drug-

resistant cancer cells as well as cancer cells pretreated with anti-cancer drugs, which are consistent with the overexpression of GST in these cells. Given that the overexpression of GST is closely associated with the development of drug resistance, these Cardipys should also hold potentials as imaging tools either to explore the drug-resistant mechanisms or screen anticancer agents that can prevent the development of drug resistance.

ASSOCIATED CONTENT

Supporting Information.

The Supporting Information is available free of charge via the Internet at http://pubs.acs.org.

Detailed experimental conditions and methods,

Supplementary data including supporting figures, ^{1}H and ^{13}C NMR and HRMS spectra.

AUTHOR INFORMATION

Corresponding Author

*guow@sxu.edu.cn and liujing4203@sxu.edu.cn

Notes

The authors declare no competing financial interest.

ACKNOWLEDGMENT

This work was supported by Natural Science Foundation of China (Nos. 21877077, 21502108, 21778036, 21904082) and Scientific Instrument Center of Shanxi University.

REFERENCES

(1) Li, X.; Gao, X.; Shi, W.; Ma, H. Design strategies for water-soluble small molecular chromogenic and fluorogenic probes. *Chem. Rev.* **2014**, *114*, 590–659.

(2) Guo, Z.; Park, S.; Yoon, J.; Shin, I. Recent progress in the development of near-infrared fluorescent probes for bioimaging applications. *Chem. Soc. Rev.* **2014**, *43*, 16–29.

(3) Yue, D.; Wang, M.; Deng, F.; Yin, W.; Zhao, H.; Zhao, X.; Xu, Z. Biomarker-targeted fluorescent probes for breast cancer imaging. *Chinese Chem. Lett.* **2018**, *29*, 648–656.

(4) Tu, L.; Xu, Y.; Ouyang, Q.; Li, X.; Sun Y. Recent advances on small-molecule fluorophores with emission beyond 1000 nm for better molecular imaging in vivo. *Chinese Chem. Lett.* **2019**, *30*, 1731–1737.

(5) van Dam, G. M.; Themelis, G.; Crane, L. M. A.; Harlaar, N. J.; Pleijhuis, R. G.; Kelder, W.; Sarantopoulos, A.; de Jong, J. S.; Arts, H. J. G.; van der Zee, A. G. J.; Bart, J.; Low, P. S.; Ntziachristos, V. Intraoperative tumor-specific fluorescence imaging in ovarian cancer by folate receptor-α targeting: first in-human results. *Nat. Med.* **2011**, *17*, 1315–1319.

(6) Wang, L.; Du, W.; Hu, Z.; Uvdal, K.; Li, L.; Huang, W. Hybrid rhodamine fluorophores in the visible–NIR region for biological imaging. *Angew. Chem. Int. Ed.* **2019**, *58*, 14026–14043.

(7) Grimm, J. B.; English, B. P.; Chen, J.; Slaughter, J. P.; Zhang, Z.; Revyakin, A.; Patel, R.; Macklin, J. J.; Normanno, D.; Singer, R. H.; Lionnet, T.; Lavis, L. D. A general method to improve fluorophores for live-cell and single-molecule microscopy. *Nat. Methods* **2015**, *12*, 244–250.

(8) Liu, X.; Qiao, Q.; Tian, W.; Liu, W.; Chen, J.; Lang, M. J.; Xu, Z. Aziridinyl fluorophores demonstrate bright fluorescence and superior photostability by effectively inhibiting twisted intramolecular charge transfer. *J. Am. Chem. Soc.* **2016**, *138*, 6960–6963.

(9) Ye, Z.; Yang, W.; Wang, C.; Zheng, Y.; Chi, W.; Liu, X.; Huang, Z.; Li, X.; Xiao, Y. Quaternary piperazine-substituted rhodamines with enhanced brightness for super-resolution imaging. *J. Am. Chem. Soc.*, **2019**, *141*, 14491–14495.

(10) Butkevich, A. N.; Bossi, M. L.; Lukinavičius, G.; Hell, S. W. Triarylmethane fluorophores resistant to oxidative photobluing. *J. Am. Chem. Soc.* **2019**, *141*, 981–989.

(11) Grzybowski, M.; Taki, M.; Senda, K.; Sato, Y.; Ariyoshi, T.; Okada, Y.; Kawakami, R.; Imamura, T.; Yamaguchi, S. A highly photostable near-infrared labeling agent based on a phospha-rhodamine for long-term and deep imaging. *Angew. Chem. Int. Ed.* **2018**, *57*, 10137 –10141.

(12) Ren, T.-B.; Xu, W.; Zhang, W.; Zhang, X.-X.; Wang, Z.-Y.; Xiang, Z.; Yuan, L.; Zhang, X.-B. A general method to increase stokes shift by introducing alternating vibronic structures. *J. Am. Chem. Soc.* **2018**, *140*, 7716–7722.

(13) Chen, W.; Xu, S.; Day, J. J.; Wang, D.; Xian, M. A general strategy for development of near-infrared fluorescent probes for bioimaging. *Angew. Chem. Int. Ed.* **2017**, *56*, 16611–16615.

(14) Liu, J.; Sun, Y.-Q.; Zhang, H.; Shi, H.; Shi, Y.; Guo, W. Sulfone-rhodamines: a new class of near-infrared fluorescent dyes for bioimaging. *ACS Appl. Mater. Interfaces* **2016**, *8*, 22953−22962.

(15) Lv, X.; Gao, C.; Han, T.; Shi H.; Guo, W. Improving the quantum yields of fluorophores by inhibiting twisted intramolecular charge transfer using electron-withdrawing group-functionalized piperidine auxochromes. *Chem. Commun.* **2020**, *56*, 715–6718.

(16) Benson, S.; Fernandez, A.; Barth, N. D.; de Moliner, F.; Horrocks, M. H.; Herrington, C. S.; Abad, J. L.; Delgado, A.; Kelly, L.; Chang, Z.; Feng, Y.; Nishiura, M.; Hori, Y.; Kikuchi, K.; Vendrell, M. SCOTfluors: small, conjugatable, orthogonal and tunable fluorophores for *in vivo* imaging of cell metabolism. *Angew. Chem. Int. Ed.* **2019**, *58*, 6911–6915.

(17) Treibs, A.; Kreuzer, F. H. Difluorboryl-Komplexe von Di- und Tripyrrylmethenen. *Justus Liebigs Ann. Chem.* **1968**, *718*, 208–223.

(18) Loudet A.; Burgess, K. BODIPY dyes and their derivatives: syntheses and spectroscopic properties. *Chem. Rev.* **2007**, *107*, 4891–4932.

(19) Ulrich, G.; Ziessel, R.; Harriman, A. The chemistry of fluorescent bodipy dyes: versatility unsurpassed. *Angew. Chem. Int. Ed.* **2008**, *47*, 1184 –1201.

(20) Boens, N.; Leen, V.; Dehaen, W. Fluorescent indicators based on BODIPY. *Chem. Soc. Rev.* **2012**, *41*, 1130–1172.

(21) Kowad, T.; Maeda, H.; Kikuchi, K. BODIPY-based probes for the fluorescence imaging of biomolecules in living cells. *Chem. Soc. Rev.* **2015**, *44*, 4953–4972.

(22) Lu, H.; Mack, J.; Yang, Y.; Shen, Z. Structural modification strategies for the rational design of red/NIR region BODIPYs. *Chem. Soc. Rev.* **2014**, *43*, 4778–4823.

(23) Liu, M.; Ma, S.; She, M.; Chen, J.; Wang, Z.; Liu, P.; Zhang, S.; Li, J. Structural modification of BODIPY: Improve its applicability. *Chinese Chem. Lett.* **2019**, *30*, 1815–1824.

(24) Kamkaew, A.; Lim, S. H.; Lee, H. B.; Kiew, L. V.; Chung, L. Y.; Burgess, K. BODIPY dyes in photodynamic therapy. *Chem. Soc. Rev.* **2013**, *42*, 77–88.

(25) Sun, W.; Zhao, X.; Fan, J.; Du, J.; Peng, X. Boron dipyrromethene nano-photosensitizers for anticancer phototherapies. *Small* **2019**, *15*, 1804927.

(26) Zhao, J.; Xu, K.; Yang, W.; Wang, Z.; Zhong, F. The triplet excited state of Bodipy: formation, modulation and application. *Chem. Soc. Rev.* **2015**, *44*, 8904–8939.

(27) Li, L.; Han, J.; Nguyen, B.; Burgess, K. Syntheses and spectral properties of functionalized, water-soluble bodipy derivatives. *J. Org. Chem.* **2008**, *73*, 1963–1970.

(28) Niu, S. L.; Ulrich, G.; Ziessel, R.; Kiss, A.; Renard, P.-Y.; Romieu, A. Water-soluble BODIPY derivatives. *Org. Lett.* **2009**, *11*, 2049–2052.

(29) Courtis, A. M.; Santos, S. A.; Guan, Y.; Hendricks, J. A.; Ghosh, B.; Szantai-Kis, D. M.; Reis, S. A.; Shah, Mazitschek, J. V.; Monoalkoxy, R. BODIPYs—A fluorophore class for bioimaging. *Bioconjugate Chem.* **2014**, *25*, 1043–1051.

(30) Fihey, A.; Favennec, A.; Guennic, B. L.; Jacquemin, D. Investigating the properties of PODIPYs (phosphorus-dipyrromethene) with ab initio Tools. *Phys. Chem. Chem. Phys.* **2016**, *18*, 9358–9366.

(31) Franke, J. M.; Raliski, B. K.; Boggess, S. C.; Natesan, D. V.; Koretsky, E. T.; Zhang, P.; Kulkarni, R. U.; Deal, P.E.; Miller, E. W. BODIPY fluorophores for membrane potential imaging. *J. Am. Chem. Soc.* **2019**, *141*, 12824–12831.

(32) Kand, D.; Liu, P.; Navarro, M. X.; Fischer, L. J.; Rousso-Noori, L.; Friedmann-Morvinski, D.; Winter, A. H.; Miller, E. W.; Weinstain, R. Water-soluble BODIPY photocages with tunable cellular localization. *J. Am. Chem. Soc.* **2020**, *142*, 4970–4974.

(33) Atilgan, S.; Ekmekci, Z.; Dogan, A. L.; Guc, D.; Akkaya, E. U. Water soluble distyryl-boradiazaindacenes as efficient photosensitizers for photodynamic therapy. *Chem. Commun.* **2006**, *42*, 4398–4400.

(34) Zhu, S.; Zhang, J.; Vegesna, G.; Luo, F.-T.; Green, S. A.; Liu, H. Highly water-soluble neutral BODIPY dyes with controllable fluorescence quantum yields. *Org. Lett.* **2011**, *13*, 438–441.

(35) Murtagh, J.; Frimannsson, D. O.; O'Shea, D. F. Azide conjugatable and pH responsive near-infrared fluorescent imaging probes. *Org. Lett.* **2009**, *11*, 5386–5389.

(36) Lv, H.; Zhang, X.; Wang, S.; Xing, G. Assembly of BODIPY-carbazole dyes with liposomes to fabricate fluorescent nanoparticles for lysosomal bioimaging in living cells. *Analyst* **2017**, *142*, 603–607.

(37) Cheng, M. H. Y.; Harmatys, K. M.; Charron, D. M.; Chen, J.; Zheng, G. Stable J-aggregation of an aza-BODIPY-lipid in a liposome for optical cancer imaging. *Angew. Chem. Int. Ed.* **2019**, *58*, 13394–13399.

(38) Taylor-Pashow, K. M. L.; Rocca, J. D.; Xie, Z.; Tran, S.; Lin, W. Postsynthetic modifications of iron-carboxylate nanoscale metal-organic frameworks for imaging and drug delivery. *J. Am. Chem. Soc.* **2009**, *131*, 14261–14263.

(39) Sharker, S. M.; Kang, E. B.; Shin, C.-I.; Kim, S. H.; Lee, G.; Park, S. Y. Near-infrared-active and pH-responsive fluorescent polymer-integrated hybrid graphene oxide nanoparticles for the detection and treatment of cancer. *J. Appl. Polym. Sci.* **2016**, *133*, 43791.

(40) Wang, Z.; Huang, L.; Yan, Y.; El-Zohry, A. M.; Toffoletti, A.; Zhao, J.; Barbon, A.; Dick, B.; Mohammed, O. F.; Han, G. Deciphering the intersystem crossing in a helical BODIPY for recorded low dose photodynamic therapy. *Angew. Chem. Int. Ed.* **2020**, *59*, 16114–16121.

(41) Kolmakov, K.; Belov, V. N.; Wurm, C. A.; Harke, B.; Leutenegger, M.; Eggeling, C.; Hell, S. W. A versatile route to red-emitting carbopyronine dyes for optical microscopy and nanoscopy. *Eur. J. Org. Chem.* **2010**, *19*, 3593–3610.

(42) Kolmakov, K.; Wurm, C.; Sednev, M. V.; Bossi, M. L.; Belov, V. N.; Hell, S. W. Masked red-emitting carbopyronine dyes with photosensitive 2-diazo-1-indanone caging group. *Photochem. Photobiol. Sci.* **2012**, *11*, 522–532.

(43) Jeon, S.; Kim, T.-I.; Jin, H.; Lee, U.; Bae, J.; Bouffard, J.; Kim, Y. Amine-reactive activated esters of *meso*-carboxyBODIPY: fluorogenic assays and labeling of amines, amino acids, and proteins. *J. Am. Chem. Soc.* **2020**, *142*, 9231–9239.

(44) Oushiki, D.; Kojima, H.; Terai, T.; Arita, M.; Hanaoka, K.; Urano, Y.; Nagano, T. Development and application of a near-infrared fluorescence probe for oxidative stress based on differential reactivity of linked cyanine dyes. *J. Am. Chem. Soc.* **2010**, *132*, 2795–2801.

(45) Johnson, L. V.; Walsh, M. L.; Chen, L. B. Localization of mitochondria in living cells with rhodamine 123. *Proc. Natl. Acad. Sci. U. S. A.* **1980**, *77*, 990−994.

(46) Xu, Z.; Xu, L. The fluorescent probes for the selective detection of chemical species inside mitochondria. *Chem. Commun.* **2016**, *52*, 1094–1119.

(47) Wang, J.; Zhu, X.; Zhang, J.; Wang, H.; Liu, G.; Bu, Y.; Yu, J.; Tian, Y.; Zhou, H. AIE based theranostic agent: *in-situ* tracking mitophagy prior to late apoptosis to guide the photodynamic therapy. *ACS Appl. Mater. Interfaces* **2020**, *12*, 1988–1996.

(48) Luzio, J. P.; Pryor, P. R.; Bright, N. A. Lysosomes: fusion and function. *Nat. Rev. Mol. Cell Biol.* **2007**, *8*, 622–632.

(49) Saftig, P.; Klumperman, J. Lysosome biogenesis and lysosomal membrane proteins: trafficking meets function. *Nat. Rev. Mol. Cell Biol.* **2009**, *10*, 623–635.

(50) Lincoln, R.; Greene, L. E.; Zhang, W.; Louisia, S.; Cosa, G. Mitochondria alkylation and cellular trafficking mapped with a lipophilic BODIPY−acrolein fluorogenic probe. *J. Am. Chem. Soc.* **2017**, *139*, 16273–16281.

(51) Fujikawa, Y.; Urano, Y.; Komatsu, T.; Hanaoka, K.; Kojima, H.; Terai, T.; Inoue, H.; Nagano, T. Design and synthesis of highly sensitive fluorogenic substrates for glutathione S-transferase and application for activity imaging in living cells. *J. Am. Chem. Soc.* **2008**, *130*, 14533–14543.

(52) Ott, M.; Gogvadze, V.; Orrenius, S.; Zhivotovsky, B. Mitochondria, oxidative stress and cell death. *Apoptosis* **2007**, *12*, 913–922.

(53) Winyard, P. G.; Moody, C. J.; Jacob, C. Oxidative activation of antioxidant defence. *Trends Biochem. Sci.* **2005**, *30*, 453–461.

(54) Lee, M. H.; Park, N.; Yi, C.; Han, J. H.; Hong, J. H.; Kim, K. P.; Kang, D. H.; Sessler, J. L.; Kang, C.; Kim, J. S. Mitochondria-immobilized pH-sensitive Off-On fluorescent probe. *J. Am. Chem. Soc.*, **2014**, *136*, 14136–14142.

(55) Johansson, L.; Gafvelin, G.; Arnér, E. S. J. Selenocysteine in proteins–properties and biotechnological use. *Biochimica et Biophysica Acta* **2005**, *1726*, 1–13.

(56) Tew, K. D.; Townsend, D. M. Glutathione-S-transferases as determinants of cell survival and death. *Antioxid. Redox Sign.* **2012**, *17*, 1728–1737.

(57) Hayes, J. D.; Flanagan, J. U.; Jowsey, I. R. Glutathione transferases. *Annu. Rev. Pharmacol. Toxicol.* **2005**. *45*, 51–88.

(58) Graminski, G. F.; Kubo, Y.; Armstrong, R. N. Spectroscopic and kinetic evidence for the thiolate anion of glutathione at the active site of glutathione S-transferase. *Biochemistry* **1989**, *28*, 3562–3568.

(59) Alary, J.; Fernandez, Y.; Debrauwer, L.; Perdu, E.; Guéraud, F. Identification of intermediate pathways of 4-hydroxynonenal metabolism in the rat. *Chem. Res. Toxicol.* **2003,** *16,* 320–327.

(60) Yang, J.; Tallman, K. A.; Porter, N. A.; Liebler, D. C. Quantitative chemoproteomics for site-specific analysis of protein alkylation by 4-hydroxy-2-nonenal in cells. *Anal. Chem.* **2015**, *87*, 2535–2541.

(61) Sau, A.; Tregno, F. P.; Valentino, F.; Federici, G.; Caccuri, A.M. Glutathione transferases and development of new principles to overcome drug resistance. *Arch. Biochem. Biophys.*, **2010**, *500*, 116–122.

(62) Kaur, G.; Gupta, S. K.; Singh, P.; Ali, V.; Kumar, V.; Verma, M. Drug metabolizing enzymes: role in drug resistance in cancer. *Clin. Transl. Oncol.* **2020**, *22*, 1667–1680.

(63) McIlwain, C. C.; Townsend D. M.; Tew, K. D. Glutathione S-transferase polymorphisms: cancer incidence and therapy. *Oncogene* **2006**, *25*, 1639–1648.

(64) Caffrey, P. B.; Zhu, M.; Zhang, Y.; Chinen, N.; Frenkel, G. D. Rapid development of glutathione-S-transferase-dependent drug resistance in vitro and its prevention by ethacrynic acid. *Cancer Lett.* **1999**, *136*, 47–52.

(65) Anderson, M. F.; Nilsson, M.; Sims, N. R. Glutathione monoethylester prevents mitochondrial glutathione depletion during focal cerebral ischemia. *Neurochem. Int.* **2004**, *44*, 153–159.

(66) Ogunrinu, T. A.; Sontheimer, H.. Hypoxia increases the dependence of glioma cells on glutathione. *J. Biol. Chem.* **2010**, *285*, 37716–37724.

(67) Perluigi, M.; Coccia, R.; Butterfield, D. A. 4-Hydroxy-2-nonenal, a reactive product of lipid peroxidation, and neurodegenerative diseases: a toxic combination illuminated by redox proteomics studies. *Antioxid. Redox Signaling* **2012**, *17*, 1590−1609.

(68) Shibata, T.; Shimozu, Y.; Wakita, C.; Shibata, N.; Kobayashi, M.; Machida, S.; Kato, R.; Itabe, H.; Zhu, X.; Sayre, L. M.; Uchida, K. Lipid peroxidation modification of protein generates *n*-(4-oxononanoyl)lysine as a pro-inflammatory ligand. *J. Biol. Chem.* **2011**, *286*, 19943−19957.

SYNOPSIS TOC (Word Style "SN_Synopsis_TOC").